Scientific Research Publishing

Journal of Biosciences and Medicines, 2023, 11, 177-185
https://www.scirp.org/journal/jbm
ISSN Online: 2327-509X
ISSN Print: 2327-5081

Numerical Modeling and Computer Simulation of a Meander Line Antenna for Alzheimer's Disease Treatment, a Feasibility Study

Felipe P. Perez[1], Maryam Rahmani[2], Jorge Morisaki[3], Farhan Amran[2], Syazwani Bakri[2], Akmal Halim[3], Alston Dsouza[2], Nurafifi Mohd Yusuff[2], Amran Farhan[2], James Maulucci[2], Maher Rizkalla[2]

[1]Department of Medicine, Division of General Internal Medicine and Geriatrics, Indiana University School of Medicine, Indianapolis, USA
[2]Department of Electrical and Computer Engineering, Indiana University-Purdue University, Indianapolis, USA
[3]Department of Bioengineering, University of Illinois at Chicago, Chicago, USA
Email: mrizkall@iupui.edu

How to cite this paper: Perez, F.P., Rahmani, M., Morisaki, J., Amran, F., Bakri, S., Halim, A., Dsouza, A., Yusuff, N.M., Farhan, A., Maulucci, J. and Rizkalla, M. (2023) Numerical Modeling and Computer Simulation of a Meander Line Antenna for Alzheimer's Disease Treatment, a Feasibility Study. *Journal of Biosciences and Medicines*, **11**, 177-185.
https://doi.org/10.4236/jbm.2023.112013

Received: December 30, 2022
Accepted: February 14, 2023
Published: February 17, 2023

Abstract

Alzheimer's disease (AD) is a brain disorder that eventually causes memory loss and the ability to perform simple cognitive functions; research efforts within pharmaceuticals and other medical treatments have minimal impact on the disease. Our preliminary biological studies showed that Repeated Electromagnetic Field Stimulation (REFMS) applying an EM frequency of 64 MHz and a specific absorption rate (SAR) of 0.4 - 0.9 W/kg decrease the level of amyloid-β peptides (Aβ), which is the most likely etiology of AD. This study emphasizes uniform E/H field and SAR distribution with adequate penetration depth penetration through multiple human head layers driven with low input power for safety treatments. In this work, we performed numerical modeling and computer simulations of a portable Meander Line antenna (MLA) to achieve the required EMF parameters to treat AD. The MLA device features a low cost, small size, wide bandwidth, and the ability to integrate into a portable system. This study utilized a High-Frequency Simulation System (HFSS) in the design of the MLA with the desired characteristics suited for AD treatment in humans. The team designed a 24-turn antenna with a 60 cm length and 25 cm width and achieved the required resonant frequency of 64 MHz. Here we used two numerical human head phantoms to test the antenna, the MIDA and spherical head phantom with six and seven tissue layers, respectively. The antenna was fed from a 50-Watt input source to obtain the SAR of 0.6 W/kg requirement in the center of the simulated brain tissue layer. We found that the E/H field and SAR distribution produced was not homogeneous; there were areas of high SAR values close to the antenna transmitter,

also areas of low SAR value far away from the antenna. This paper details the antenna parameters, the scattering parameters response, the efficiency response, and the E and H field distribution; we presented the computer simulation results and discussed future work for a practical model.

Keywords

Alzheimer's Disease, Meander Line Antenna, HFSS, EMF Linearity, SAR, Field Distribution

1. Introduction

Small size antennas have been the focus of cellular communication systems, bioinstrumentations, medical and IoT devices. This is due to high demand of the compact equipment. The small size antennas in medical applications are suited for use in and around human bodies. There are multiple antenna approaches [1] [2] [3] [4] for the E/H linearity within the human body, while lacks the portable size feature that enables integrating them around the human tissue sizes. The rapid development in devices that emit Radio Frequency Electromagnetic Fields (RF-EMF) has sparked a growing interest in their interaction with biological systems and their beneficial effects on human health. As a result, investigations are motivated by the potential for therapeutic applications and concern for any possible side effects of these EM energies. Some studies have indicated that a specific tuning of experimental and clinical Radio Frequency (RF) exposure may lead to their clinical application toward beneficial health outcomes.

Figure 1 shows the block diagram of the proposed system. The function generator will provide the EM power required to transmit the appropriate SAR in the brain layer. The antenna will radiate and focus the EM energy in the human head phantom direction. The antenna position will be on top of the head phantom. The head phantom will simulate a real human head with 5 tissue layers, EMF exposure will reach a SAR of 0.4 - 0.9 W/kg in the brain layer.

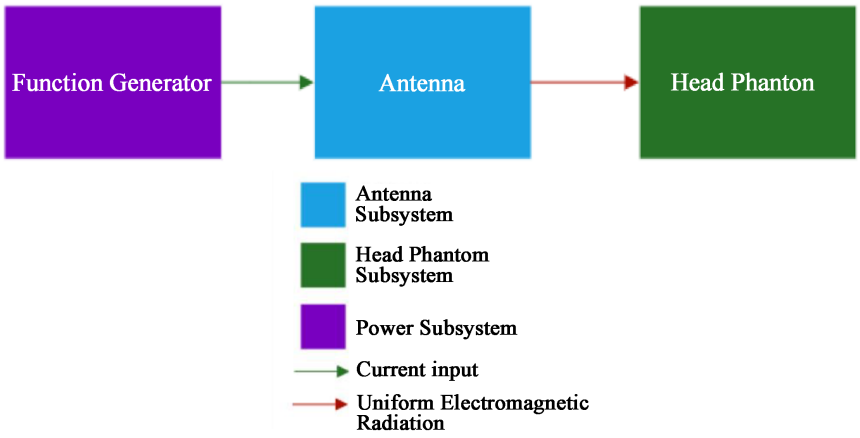

Figure 1. System block diagram.

The application investigated here is the near zone field distribution for HF/VHF antenna since the human head is placed very close to the antenna surface. The study of near zone field has been investigated and measured for their linear distribution [5] [6]. The size of the antenna to perform at 64 MHZ (VHF) is important for wearable devices. The design has been implemented for 64 MHZ while the size of the antenna was beyond the wearing device limitation [7].

2. Antenna Design

We chose the Meander Line Antenna (MLA) for this design [8] [9], because the antenna size is suitable for a portable system and satisfies the AD treatment SAR requirements. Figure 2 shows the geometry, and Table 1 shows the detailed dimensions of the antenna.

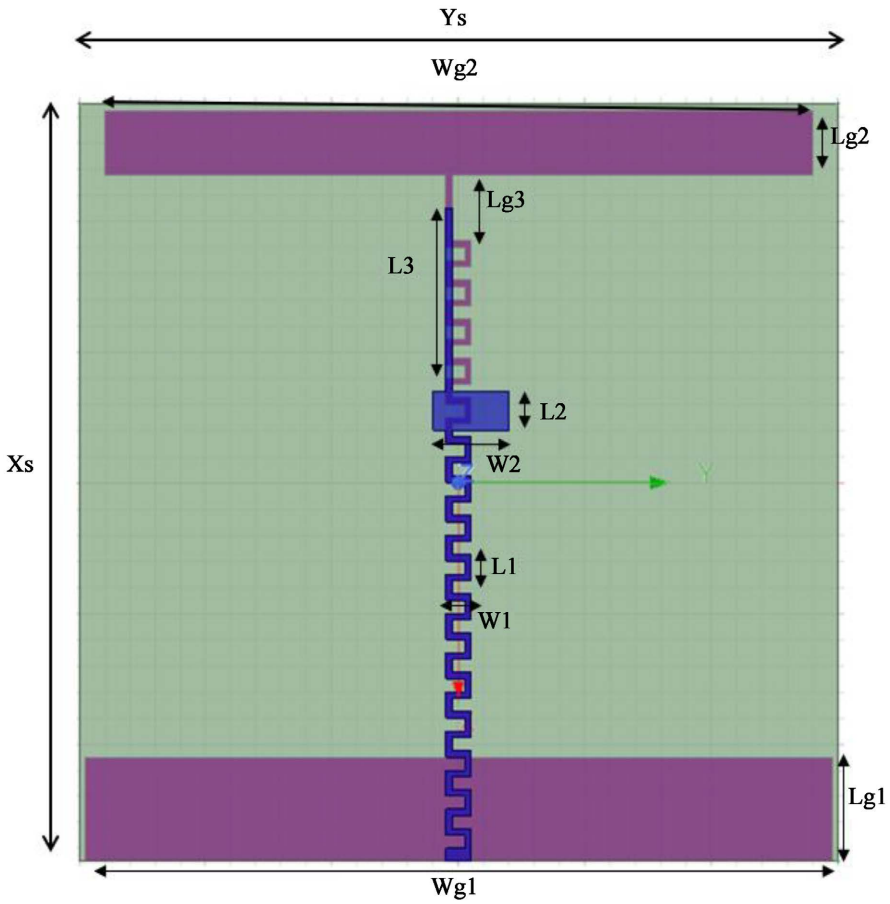

Figure 2. Geometry of the meander monopole line antenna.

Table 1. Dimensions of the meander monopole line antenna.

Xs	58.0 cm	**Wg2**	56.0 cm	**L2**	3.0 cm
Ys	60.0 cm	**Lg2**	5.0 cm	**W2**	6.0 cm
Wg1	59.0 cm	**L1**	2.0 cm	**L3**	14.0 cm
Lg1	8.0 cm	**W1**	2.0 cm	**Lg3**	7.0 cm

Table 2 shows the dimensions of the various layers within the human head phantom and the dielectric properties of each layer. The parameters in Table 2 were incorporated into the HFSS simulation system for the antenna radiation at the given frequency. The material of the substrate is Rogers RO30130 which has a high dielectric value of 10.2 that allows the antenna to obtain a higher gain within the human head phantom direction. The number of meander turns also affects the radiation frequency. The number of turns for the meander line of ground is 27 turns and 21 turns for the top patch.

3. The Head Phantom Models

In this study, we performed two different simulation head phantom models, the Multimodal Imaging-Based Detailed Anatomical Model of the Human Head and Neck (MIDA), and the Spherical Model Head Phantom.

Both head phantoms were based on the parameters stated in Table 2.

4. Results and Discussion

4.1. Antenna and MIDA Head Phantom

Figure 3 shows the Scattering S_{11} parameters of the resonating frequency of 64 MHz, and Figure 4 shows the SAR distribution in the MIDA human head phantom. Table 3 shows the minimum and maximum SAR observed in the various layers before reaching the brain layer; the SAR in the brain layer in blue color was between 0.9 and 0.0024 W/kg. We observed that the nonlinearity was an issue with this antenna exposure on the human head phantom model.

Within the five different layers of surfaces simulated for the SAR values for the MIDA [10] head phantom, the skin appeared to have a very high average SAR value because it is the closest surface to the antenna radiation. We observed that the power was dissipated in the skin before the radiation reached the skull. The values of the SAR across the head phantom are relatively not linear. One possible cause is that the source of the EMF radiation is on top of the head and the SAR decreases with increasing distance from the antenna. The other cause is

Table 2. Properties of the Seven Different Layers of the Brain at a frequency of 64 MHz.

Layer	Radius (mm)	Permittivity (e_r)	Permeability	Conductivity (S/m)	Mass Density (kg/m^3)
Skin	51.0	32	1	0.1483	1109.0
Fat	49.0	9	1	0.0776	0911.0
Muscle	47.0	50	1	0.4466	1090.4
Skull	45.0	10	1	0.0179	1908.0
Dura	36.5	40	1	0.0600	1174.0
CSF	36.0	65	1	1.8790	1007.0
Brain	28.1	40	1	0.6165	1045.5

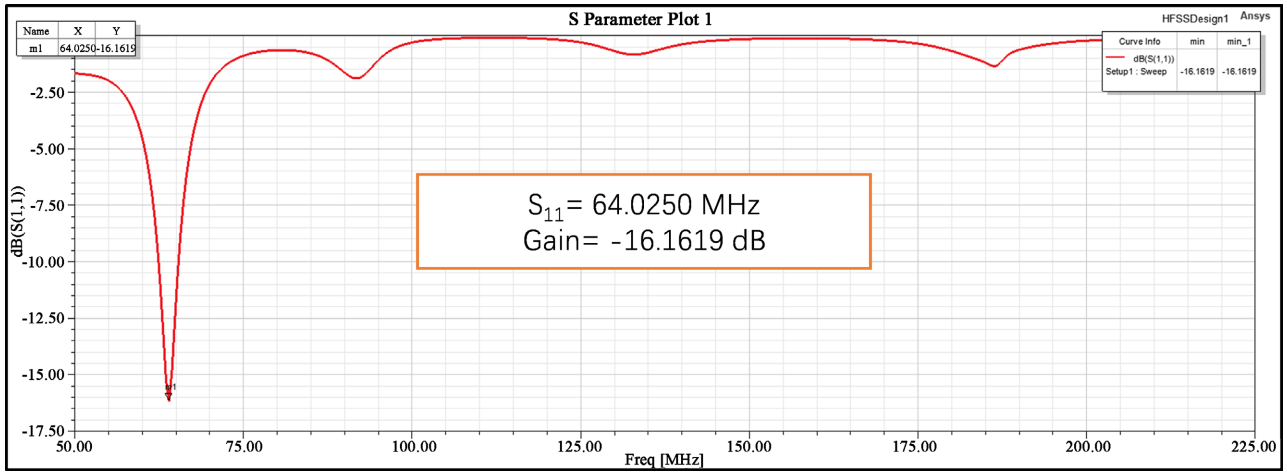

Figure 3. S_{11} Parameter VS gain graph of the antenna.

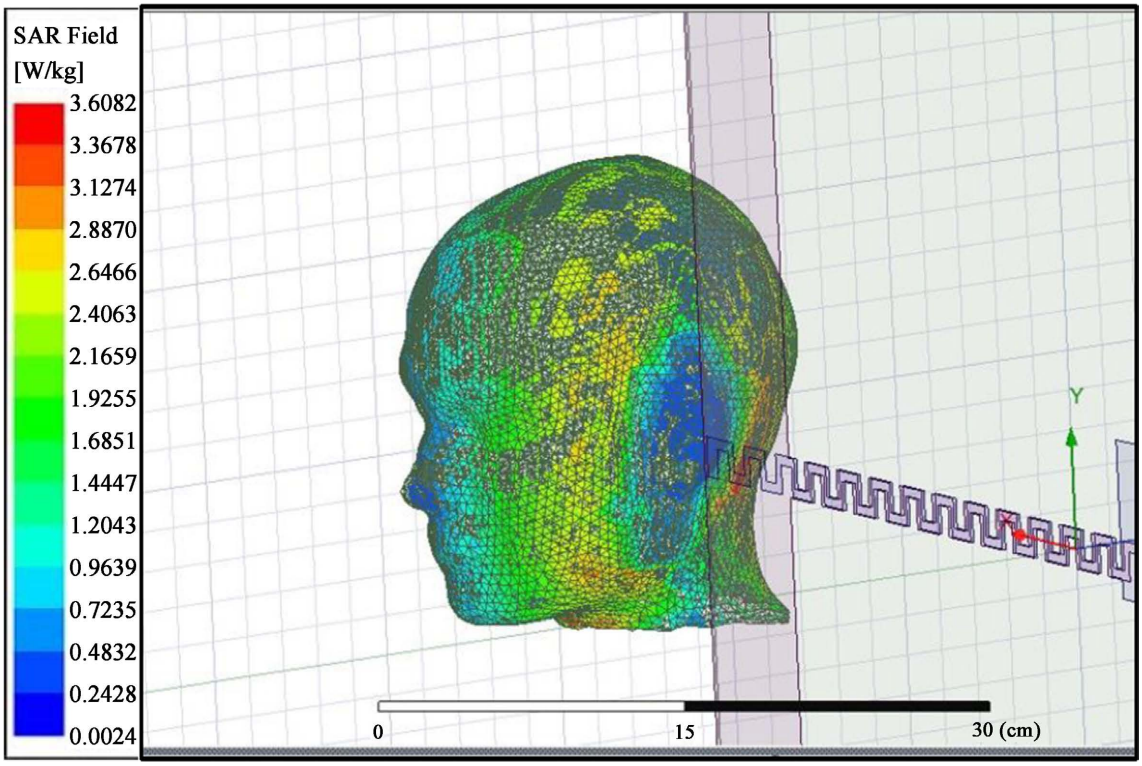

Figure 4. SAR result on the MIDA human head phantom.

Table 3. Tabulated data of average SAR in the different layers of the MIDA human head phantom.

Layers	Max. Value of Average SAR (W/kg)	Min. Value of Average SAR (W/kg)
Skin	3.6082	0.0264
Skull	2.8870	0.0261
Dura	1.2043	0.0104
CSF	2.1669	0.0303
Brain	0.9639	0.0024

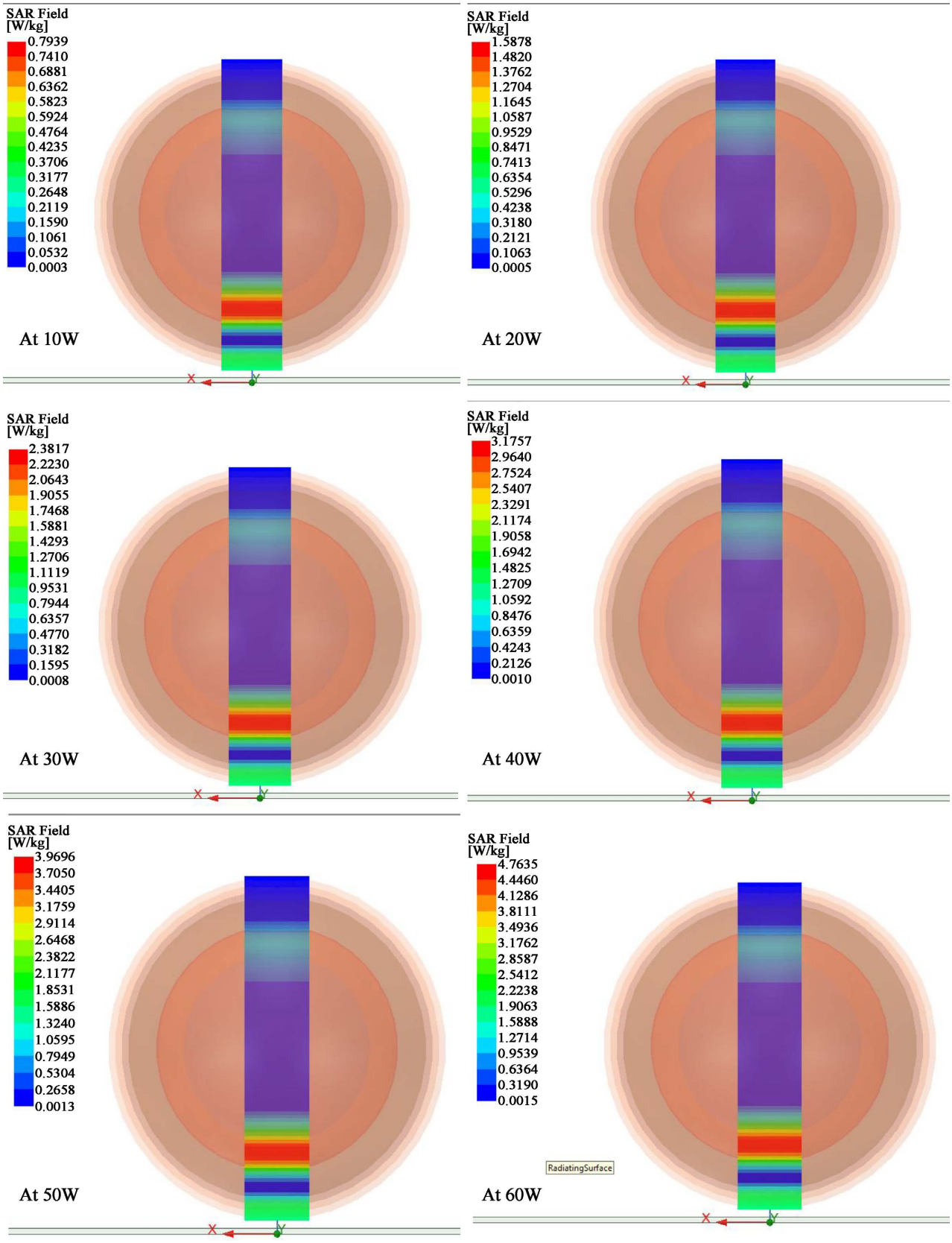

Figure 5. SAR field with various power applied. We determined that the 30 W, 40 W, 50 W and 60 W produced a SAR between 0.4 and 0.9 W/kg (see **Table 4**) in the center of the simulated brain layer (in purple color).

that the SAR is calculated based on the mass density of each layer and not on the whole head. This causes some errors in the SAR value and produces a non-homogeneous distribution of the SAR values in each layer. For example, the SAR values in the brain layer are between 0.0024 and 0.9639 W/kg, therefore showing areas of the brain with insufficient energy to produce biological effects. The inconsistency of the SAR values is also due to the complex structure of the MIDA head phantom with complex boundaries between layers.

4.2. Antenna and Spherical Model Head Phantom

We utilized the same MLA antenna to perform EMF exposures to the spherical model head phantom with the S11 parameters. We tried several power levels until we reached the appropriate SAR of 0.4 - 0.9 W/kg. Figure 5 gives the SAR distribution for two different power values; 1 W and 50 W. Table 4 shows the SAR versus power generated and fed into the antenna. We reached a SAR of 0.6 W/kg at the brain tissue of the human head phantom using a power of 50 W.

The average SAR is higher in the layers near the antenna and decreases as the distance increases. These results were expected as the tissues absorbed the energy of the radiation emitted by the antenna. When the power of the antenna is manipulated, we can observe that the distribution pattern of the average SAR is kept constant on each layer of the tissue.

5. Conclusion & Future Work

In this work, we have demonstrated that the MLA antennas are suitable for portable devices and for producing a SAR of 0.4 - 0.9 W/kg in the simulated human brain within reasonable dimensions. The study was based on a near-field distribution. The HFSS simulation showed a scattering parameter S_{11} at 64 MHZ while

Table 4. Average SAR in the simulated brain layer. We increased the power to 50 W to reach a SAR of 0.63 - 0.95 W/kg in the simulated brain.

Power (W)	Average SAR (W/kg)	Median Value (W/kg)
1	0.0113 - 0.0170	0.01415
10	0.1061 - 0.1590	0.13255
20	0.2121 - 0.3180	0.26505
30	0.3182 - 0.4770	0.39760
40	0.4243 - 0.6359	0.53010
50	0.5304 - 0.7929	0.66165
60	0.6364 - 0.9539	0.79515
70	0.7425 - 1.1129	0.9277
80	0.8486 - 1.2719	1.06025
90	0.9437 - 1.4309	1.1873
100	1.0607 - 1.5898	1.32525

keeping the antenna size within the portable range. The two head phantom models studied here show that the spherical model gives accurate data and better linearity; this is caused by the complex mathematical model of the MIDA phantom and the software capacity to handle it. Here we also determined that the SAR values decreased in tissues farthest from the antenna transmitter and produced a non-homogeneous distribution pattern which is not appropriate for future AD treatments unless we use two or more antennas to obtain a more homogeneous SAR distribution. A practical model is needed to confirm the HFSS data model, we will reserve the practical model for future consideration [11] [12].

Acknowledgements

The authors offer their appreciation to the senior design administrators and to Ms. Seemein Shayesteh, the instructor of the senior design course, for their follow-up with this work during the 2022 academic year.

Conflicts of Interest

The authors declare no conflicts of interest regarding the publication of this paper.

References

[1] Dytioco Santos, J.P., Fereidoony, F., Hedayati, M. and Wang, Y.E. (2020) High Efficiency Bandwidth VHF Electrically Small Antennas through Direct Antenna Modulation. *IEEE Transactions on Microwave Theory and Techniques*, **68**, 5029-5041, https://doi.org/10.1109/TMTT.2020.3016381

[2] Rodriguez, V. (2018) On Selecting the Most Suitable Range for Antenna Measurements in the VHF-UHF Range. 2018 *IEEE Conference on Antenna Measurements & Applications* (*CAMA*), Sweden, 3-6 September 2018, 1-3. https://doi.org/10.1109/CAMA.2018.8530667

[3] Perez, F.P., Rahmani, M., Emberson, J., Weber, M., Morisaki, J., Amran, F., Bakri, S., Halim, A., Dsouza, A., Yusuff, N.M., Farhan, A., Maulucci, J. and Rizkalla, M. (2022) EMF Antenna Exposure on a Multilayer Human Head Simulation for Alzheimer Disease Treatments. *Journal of Biomedical Science and Engineering*, **15**, 129-139. https://doi.org/10.4236/jbise.2022.155013

[4] Rubtsova, N., Perov, S., Belaya, O., Kuster, N. and Balzano, Q. (2015) Near-Field Radiofrequency Electromagnetic Exposure Assessment. *Electromagnetic Biology and Medicine*, **34**, 180-182. https://doi.org/10.3109/15368378.2015.1076444

[5] Choi, J. and Sarabandi, K. (2016) HF/VHF Antenna Characterization from Very-near-Field Measurements over Arbitrary Closed Surfaces. 2016 *United States National Committee of URSI National Radio Science Meeting* (*USNC-URSI NRSM*), Boulder, 6-9 January 2016, 1-2. https://doi.org/10.1109/USNC-URSI-NRSM.2016.7436254

[6] Villers, S. and Malhage, A. (2014) VHF Probes for Antenna Measurement in a Near Field Range. 2014 *IEEE Conference on Antenna Measurements & Applications* (*CAMA*), Antibes Juan-les-Pins, 16-19 November 2014, 1-4. https://doi.org/10.1109/CAMA.2014.7003430

[7] Perez, F.P., Bandeira, J.P., Morisaki, J.J., Peddinti, S.V.K., Salama, P., Rizkalla, J. and Rizkalla, M.E. (2017) Antenna Design and SAR Analysis on Human Head Phantom Simulation for Future Clinical Applications. *Journal of Biomedical Science and Engineering*, **10**, 421-430. https://doi.org/10.4236/jbise.2017.109032

[8] Ma, M.J. (2010) The Study and Implementation of Meadler-Line Antenna for Integrated Transceiver Design. https://www.diva-portal.org/smash/get/diva2:299692/FULLTEXT01.pdf

[9] Misman, D., Abd. Aziz, M.Z.A., Husain, M.N. and Soh, P.J. (2009) Design of Planar Meander Line Antenna. 2009 3*rd European Conference on Antennas and Propagation*, Berlin, 23-27 March 2009, 2420-2424. https://ieeexplore.ieee.org/document/5068103

[10] Iacono, M.I., Neufeld, E., Akinnagbe, E., Bower, K., Wolf, J., Oikonomidis, I.V., Sharma, D., Lloyd, B., Wilm, B.J., Wyss, M., Pruessmann, K.P., Jakab, A., Makris, N., Cohen, E.D., Kuster, N., Kainz, W. and Angelone, L.M. (2015) MIDA: A Multimodal Imaging-Based Detailed Anatomical Model of the Human Head and Neck. *PLOS ONE*, **10**, e0124126. https://doi.org/10.1371/journal.pone.0124126

[11] Perez, F.P., Maloney, B., Chopra, N., Morisaki, J.J. and Lahiri, D.K. (2021) Repeated Electromagnetic Field Stimulation Lowers Amyloid-β Peptide Levels in Primary Human Mixed Brain Tissue Cultures. *Scientific Reports*, **11**, Article No. 621. https://doi.org/10.1038/s41598-020-77808-2

[12] Perez, F.P., Bandeira, J.P., Perez Chumbiauca, C.N., Lahiri, D.K., Morisaki, J. and Rizkalla, M. (2022) Multidimensional Insights into the Repeated Electromagnetic Field Stimulation and Biosystems Interaction in Aging and Age-Related Diseases. *Journal of Biomedical Science*, **29**, Article No. 39. https://doi.org/10.1186/s12929-022-00825-y